28. N. A. Russell, A. Horii, P. F. Smith, C. L. Darlington, D. K. Bilkey, *J. Neurophysiol.* **96**, 4 (2006).
29. N. Burgess, *Hippocampus* **18**, 1157 (2008).
30. M. E. Hasselmo, L. M. Giocomo, E. A. Zilli, *Hippocampus* **17**, 1252 (2007).
31. H. T. Blair, A. C. Welday, K. Zhang, *J. Neurosci.* **27**, 3211 (2007).

Acknowledgments: This work was supported by the NSF Career award and grants from NIH 5R01MH092925-02 and the W. M. Keck foundation. These findings were presented as two abstracts and posters at the Society for Neuroscience Meeting entitled: P. Ravassard, B. Willers, A. L. Kees, D. Ho, D. Aharoni, M. R. Mehta, "Directional tuning of place cells in rats performing a virtual landmark navigation task," *Soc. Neurosci. Abs.* no. 812.05 (2012); and A. Kees, B. Willers, P.M. Ravassard, D. Ho, D. Aharoni, M. R. Mehta, "Hippocampal rate and temporal codes in a virtual visual navigation task," *Soc. Neurosci. Abs.* no. 812.07 (2012). We thank L. Acharya, Z. Chen, and J. Moore for technical help. Author contributions: P.R., A.K., D.H., and J.C. performed data collection; B.W. and D.A.A. developed the virtual reality system; B.W. and Z.M.A. performed analysis; P.R., A.K., B.W., and Z.M.A. wrote the manuscript; P.R., A.K., B.W., D.H., D.A.A., and J.C. designed the experiment; and M.R.M. participated in all of the above.

Supplementary Materials
www.sciencemag.org/cgi/content/full/science.1232655/DC1
Materials and Methods
Figs. S1 to S21
Table S1
References

12 November 2012; accepted 16 April 2013
Published online 2 May 2013;
10.1126/science.1232655

Subangstrom Resolution X-Ray Structure Details Aquaporin-Water Interactions

Urszula Kosinska Eriksson,[1]† Gerhard Fischer,[1]*† Rosmarie Friemann,[1] Giray Enkavi,[2] Emad Tajkhorshid,[2]‡ Richard Neutze[1]‡

Aquaporins are membrane channels that facilitate the flow of water across biological membranes. Two conserved regions are central for selective function: the dual asparagine-proline-alanine (NPA) aquaporin signature motif and the aromatic and arginine selectivity filter (SF). Here, we present the crystal structure of a yeast aquaporin at 0.88 angstrom resolution. We visualize the H-bond donor interactions of the NPA motif's asparagine residues to passing water molecules; observe a polarized water-water H-bond configuration within the channel; assign the tautomeric states of the SF histidine and arginine residues; and observe four SF water positions too closely spaced to be simultaneously occupied. Strongly correlated movements break the connectivity of SF waters to other water molecules within the channel and prevent proton transport via a Grotthuss mechanism.

Aquaporins are water transport facilitators found in all kingdoms of life (*1*). They are primarily responsible for water homeostasis within living cells, although a subset of aquaporins also facilitates the flow of other small polar molecules, such as glycerol or urea. As with any membrane transport facilitator, aquaporins have evolved to be highly selective for their transported substrate without binding water so strongly that transport is inhibited. In addition to excluding hydroxide (OH^-) and hydronium (H_3O^+) ions, aquaporins must also prevent proton transport via a Grotthuss mechanism (*2*, *3*) in which protons are rapidly exchanged between hydrogen bonded water molecules.

Crystal structures of bacterial (*4*, *5*), archael (*6*), yeast (*7*), plasmodium (*8*), plant (*9*), mammalian (*10*–*12*), and human (*13*–*15*) aquaporins have established that these channels contain six transmembrane α helices and associate as homotetramers. A seventh pseudo-transmembrane helix is formed by loops B and E, which fold as aligned half-helices that insert from opposite sides of the membrane and place the conserved dual asparagine-proline-alanine (NPA) signature motif near the center of the water pore (Fig. 1). Transport specificity is defined by the aromatic and arginine selectivity filter (SF) (*16*, *17*), which is located near the extracellular pore entrance and forms the narrowest portion of the channel.

Several models accounting for the ability of aquaporins to impede the passage of protons have emerged from structural arguments (*13*), molecular dynamics (MD) investigation of water structure and dynamics (*17*, *18*), and computational studies characterizing the energetics associated with explicit transfer of protons across the channel (*19*, *20*). These studies assert different microscopic mechanisms for excluding protons, including electrostatic repulsion (*19*, *21*–*23*), configurational barriers (*17*), and desolvation penalties (*24*), and they consistently report the NPA region, where the macrodipoles of the two half-helices formed by loops B and E focus a positive electrostatic potential, as the main barrier against proton transport (*17*–*24*). This creates an electrostatic barrier to proton transport (*21*) and orients the water molecule's dipole moment near the NPA motif, such that the order of oxygen and hydrogen atoms do not support proton exchange via a Grotthuss mechanism (*17*, *18*). Although intuitively appealing, this picture does not explain why mutations within the NPA motifs that diminish this positive electrostatic barrier facilitate the transport of sodium ions, but not protons (*25*, *26*); nor is it evident why mutations within the SF can allow the channel to conduct protons (*27*, *28*).

To further examine the underlying mechanism of facilitated, selective water transport, we optimized crystals of Aqy1 (*7*), the sole aquaporin of *Pichia pastoris*, and determined its crystal structure to 0.88 Å resolution (*29*), recovering *R*-factor and R_{free} values of 10.3% and 10.7%, respectively (table S1). The electron density associated with the dual-NPA–aquaporin signature motif is illustrated in Fig. 2. At subangstrom resolution, the conformations of the two NPA asparagine residues (Asn^{112} and Asn^{224}) are uniquely assigned because the $2mF_{obs} - DF_{calc}$ electron density is delocalized across the carbon-oxygen double bond of these side chains (Fig. 2, A and B, blue mesh), whereas that for the side-chain nitrogen atom is more localized: *m* is the figure of merit, and *D* is estimated from coordinate errors. Electron density associated with Glu^{51} (fully delocalized) and Gln^{137} (partially delocalized) highlights how delocalized density can be distinguished at this resolution (fig. S1). It is noteworthy that residual $mF_{obs} - DF_{calc}$ difference electron density, from a hydrogen omit map (Fig. 2, A and B, green mesh), reveals electron clouds associated with all four proton-donor interactions of the Nδ atoms of the dual-NPA asparagine residues. H-bond donor interactions of Asn^{224}:Nδ to water molecule 6 (Wat6) (peak maximum 0.42 e/Å^3) (Fig. 2A) and to the carbonyl oxygen of Leu^{111}, as well as H-bond donor interactions of Asn^{112}:Nδ to Wat7 (peak maximum 0.48 e/Å^3) (Fig. 2B) and to the carbonyl oxygen of Leu^{223}, are all resolved. These observations confirm that H-bond donor interactions from the NPA motifs constrain the orientation of passing water molecules (*13*, *17*, *18*). No modeled water has H-bond interactions with both NPA asparagines, as is often depicted (*13*, *17*, *19*, *22*, *23*), and a water molecule at this position cannot be the critical ingredient preventing Grotthuss proton transport.

MD simulations have predicted that water molecules adopt a bipolar orientation in the two halves of the channel, such that proton-donor interactions systematically point away from the NPA region, which disfavors Grotthuss proton exchange (*13*, *17*, *18*). In the cytoplasmic half-channel, residual $mF_{obs} - DF_{calc}$ electron density

[1]Department of Chemistry and Molecular Biology, University of Gothenburg, Box 462, S-40530 Göteborg, Sweden. [2]Department of Biochemistry, College of Medicine, Center for Biophysics and Computational Biology, and Beckman Institute for Advanced Science and Technology, University of Illinois, Urbana, IL 61802, USA.
*Present address: Department of Biochemistry, University of Cambridge, CB2 1GA Cambridge, UK.
†These authors contributed equally to this work.
‡Corresponding author. E-mail: richard.neutze@chem.gu.se (R.N.); emad@life.illinois.edu (E.T.)

reveals that Wat8 donates an H bond to Wat9 (peak maximum 0.73 e/Å^3) (Fig. 2C); Wat9 to Wat10 (peak maximum 0.70 e/Å^3); Wat10 to the hydroxyl group of Tyr^{31} (peak maximum 0.79 e/Å^3), and weaker residual density suggests an H bond from Wat7 to Wat8 (peak maximum 0.30 e/Å^3). A positive peak located almost exactly between Wat6 and Wat7 (peak maximum 0.50 e/Å^3) suggests that these two waters donate an H bond to each other with approximately equal probability, which illustrates that H-bond directionality is not imposed at the very center of the channel where the positive electrostatic potential is at its maximum. The polarity of water-water H bonds in the extracellular half-channel is difficult to assign because of larger anisotropic motions of Wat5 and Wat6 (B-factors of 15.0 and 13.9 Å^2, respectively) relative to water molecules in the cytoplasmic half-channel (B-factors of 9.7 to 12.1 Å^2). Nevertheless, all assigned interactions are consistent with the proposed bipolar distribution of water-water H bonds (*13*, *17*, *18*), and this polarization does not depend on the presence of a water molecule that simultaneously accepts H bonds from both NPA asparagines.

Within the SF, His^{212} and Arg^{227} are conserved among water-selective aquaporins. The side-chain conformation of His^{212} is apparent from the stronger electron density visible for its two nitrogen atoms (Fig. 3). Residual $mF_{obs} - DF_{calc}$ electron density from a hydrogen omit map reveals that Nδ of His^{212} is protonated and donates an H bond to the carbonyl oxygen of Leu^{208} (visible at 0.42 e/Å^3), whereas Nε is not protonated (Fig. 3A), which indicates its tautomeric state (fig. S2A). Similarly, the tautomeric state of Arg^{227} (fig. S2B) can be assigned because the covalent bond from Cζ of Arg^{227} to Nη2 (the nitrogen atom closest to the water channel) is most conjugated (Fig. 3A). Consistent with this assignment, electron clouds associated with the three protons of Nε and Nη1

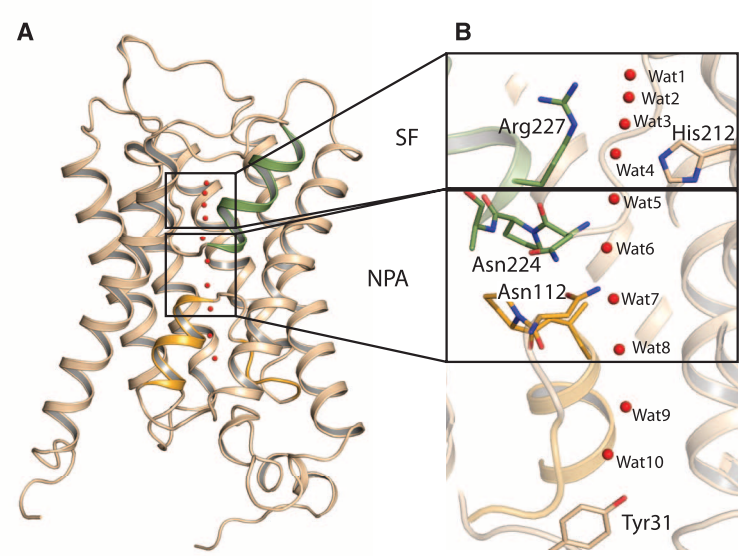

Fig. 1. Fold of Aqy1. (**A**) The six transmembrane helices and the seventh pseudo-transmembrane helix formed by loops B (orange) and E (green). (**B**) Water molecule positions within the channel (red spheres). The dual-NPA–aquaporin signature motif (bottom box) and the SF (top box) are highlighted.

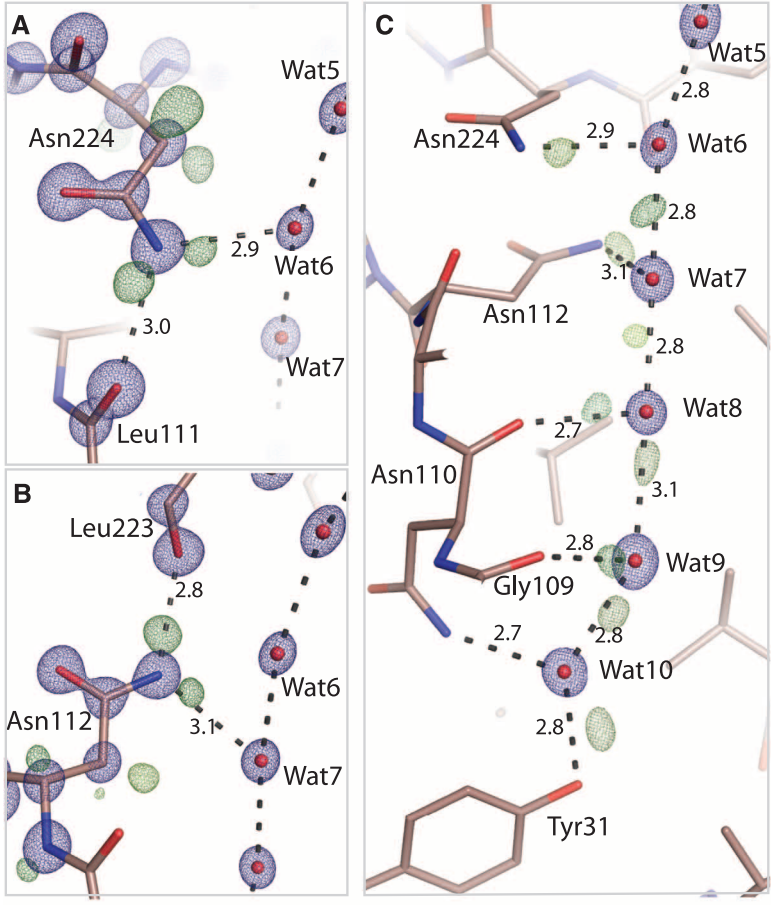

Fig. 2. Electron density within the NPA and cytoplasmic regions of the Aqy1. (**A**) The $2mF_{obs} - DF_{calc}$ (blue, contoured at 4.3 e/Å^3) and $mF_{obs} - DF_{calc}$ (green, contoured at 0.33 e/Å^3) electron density associated with Asn^{224}. (**B**) The $2mF_{obs} - DF_{calc}$ (blue, contoured at 4.3 e/Å^3) and $mF_{obs} - DF_{calc}$ (green, contoured at 0.33 e/Å3, yellow-green at 0.26 e/Å^3) electron density associated with Asn^{112}. Delocalized $2mF_{obs} - DF_{calc}$ density connects the dual-NPA asparagine Cγ and Oδ atoms, whereas that associated with Nδ is more localized. Residual $mF_{obs} - DF_{calc}$ electron density indicates H-bond donor interactions with passing water molecules. (**C**) The $2mF_{obs} - DF_{calc}$ electron density (blue, contoured at 4.3 e/Å^3) illustrates the position of water molecules, and $mF_{obs} - DF_{calc}$ residual electron density (brown-green contoured at 0.59 e/Å^3, dark green at 0.39 e/Å^3, yellow-green 0.26 to 0.33 e/Å^3, and light green contoured at 0.15 e/Å^3) indicates water H-bond interactions within the aquaporin channel.

are visible (0.48, 0.42, and 0.36 peak maxima e/Å^3, respectively) (Fig. 3A), but no residual density is visible for the protons of Nη2, presumably because the associated electrons are more tightly drawn to a net-positive charge on Nη2. This concentration of positive charge on the nitrogen atom closest to the pore maximizes the electrostatic repulsive effect of Arg^{227} on hydronium ions and thereby helps inhibit their passage.

When two water molecules were built into the electron density between His^{212} and Arg^{227} (fig. S3), they had significantly lower $2mF_{obs} - DF_{calc}$ maxima (5.0 and 5.2 e/Å^3) than all other water molecules within the aquaporin pore (~7.0 to 8.0 e/Å^3), and strong residual $mF_{obs} - DF_{calc}$ electron density peaks (maxima of 1.4 and 1.9 e/Å^3) arose adjacent to these water molecules (Fig. 3B). Placement of two additional water molecules and unrestrained refinement of their crystallographic occupancies and B-factors revealed four stable water positions within the SF with complementary occupancies of 66% (Wat2 and Wat4, $2mF_{obs} - DF_{calc}$ peak maxima of 5.2 and 5.0 e/Å^3, respectively) (Fig. 3) and 34% (Wat1 and Wat3, $2mF_{obs} - DF_{calc}$ peak maxima of 2.4 and 3.2 e/Å^3, respectively). Given their small separation (~1.5 Å) (Fig. 3A), it is not possible for all four water positions to be occupied simultaneously. Although MD simulations predict only one high-probability water position within the SF (between Wat2 and Wat3) when averaged over an entire trajectory (Fig. 4B), specific snapshots capture these crystallographic water configurations (Fig. 4, D and E) and illustrate how water molecules move pair-wise through the SF while maintaining H-bond interactions with His^{212} and Arg^{227}. This picture is analogous to the structural mechanism of ion transport through potassium channels, for which partial crystallographic occupancy of four K^+-binding sites within its selectivity filter led to the proposal that potassium ions progress pair-wise through a sequence of four binding sites (*30*, *31*). As argued for potassium channels (*31*), the similar crystallographic occupancy of the four aquaporin SF water positions implies very little energy difference between binding configurations 1,3 and 2,4, which is optimal for maximizing the water conduction rate.

Both high- and low-occupancy SF water positions have H-bond interactions with the same atoms: with Nη2 of Arg^{227} and the carbonyl oxygen of Gly^{220} for Wat1 and Wat2; and Nδ of Arg^{227}, Nε of His^{212}, and the carbonyl oxygen of Ala^{221} for Wat3 and Wat4 (Fig. 3A). MD snapshots illustrate how this geometry achieves exceptional water selectivity, because all four H-bond donor and acceptor interactions are filled as water moves through the SF (Fig. 4C). The presence of four closely spaced water-selective sites optimizes the aquaporin SF's ability to discriminate water from other small molecules. Hydroxide ions, in particular, suffer a geometric penalty, because they cannot simultaneously donate H bonds to the backbone hydroxyl of Ala^{221} and to Nε of His^{212}. Conversely, all H-bond interactions are distorted from ideal water geometry (fig. S4), and this avoids binding water too tightly, such that efficient transport is compromised.

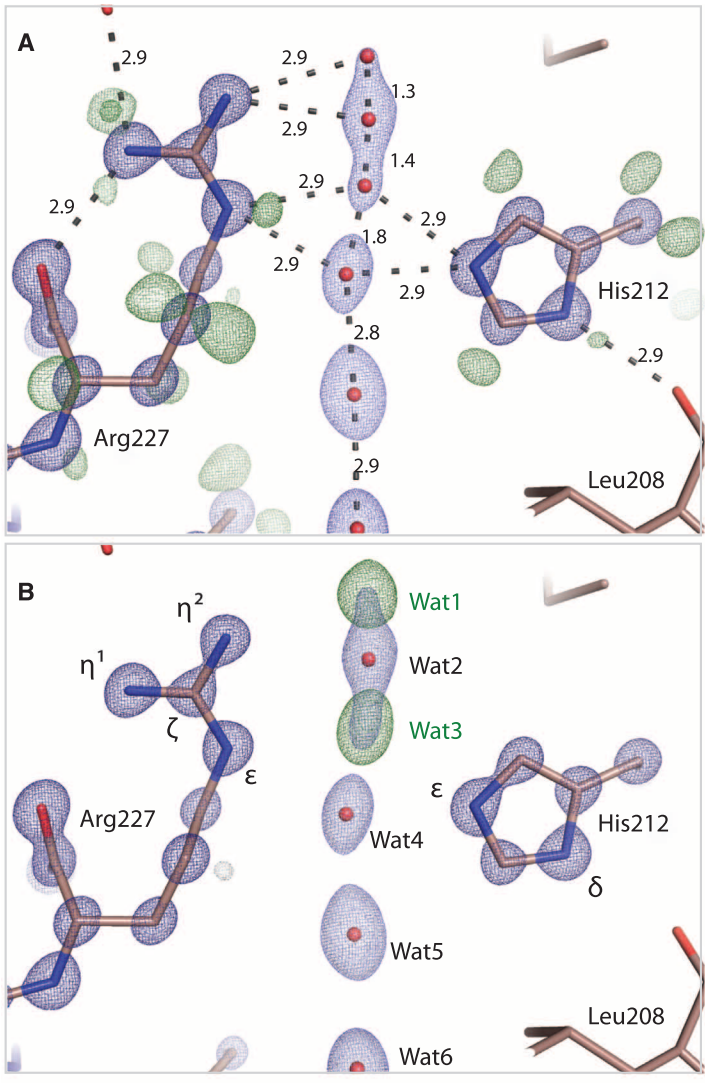

Fig. 3. Electron density within the Aqy1 SF. (**A**) The $2mF_{obs} - DF_{calc}$ (dark blue contoured at 4.3 e/Å^3 and light blue at 1.9 e/Å^3) and residual $mF_{obs} - DF_{calc}$ (dark green contoured at 0.42 e/Å^3 and light green contoured at 0.33 e/Å^3) electron density associated with His^{212}, Arg^{227}, and water molecules within the SF. Atomic separations (Å) are indicated. Residual $mF_{obs} - DF_{calc}$ electron density reveals that Nδ of His^{212} is protonated, whereas Nε is not. Connected $2mF_{obs} - DF_{calc}$ electron density suggests that the Arg^{227} covalent bond from Cζ to Nη2 is preferentially conjugated. Four closely spaced water molecules are modeled within the SF with complementary occupancy (66% occupancy, positions 2 and 4; 34% occupancy, positions 1 and 3). (**B**) The $mF_{obs} - DF_{calc}$ omit electron density map calculated when waters 1 and 3 are removed from the structural model (dark green contoured at 0.65 e/Å^3). Positive electron-density features associated with these waters are the strongest within the channel.

MD simulations reproduce the crystallographic positions of waters 5 and 7 to 10 as the most probable channel water positions at any given moment (Fig. 4A), whereas the location of Wat6 is more diffuse, consistent with its higher anisotropic crystallographic B-factor. The H-bond connectivity of water molecules is significantly perturbed at both the NPA and the SF regions of the channel, preventing Grotthuss proton transport (fig. S5). Within the NPA region, this disruption is accompanied by a reduction in the correlated motion of water molecules (Fig. 4B), because one water molecule (corresponding to Wat6) rapidly alternates its H-bond interactions between neighboring waters on either half of the channel. This finding is consistent with the crystal structure, because residual $mF_{obs} - DF_{calc}$ electron density between Wat6 and Wat7 is significantly weaker than that observed between waters 8, 9 and 10, and no residual density is visible between Wat5 and Wat6 to suggest a well-defined H bond (Fig. 2C). In contrast, water molecules move pair-wise through the SF in a highly correlated manner (Fig. 4B), and their connectivity to water molecules

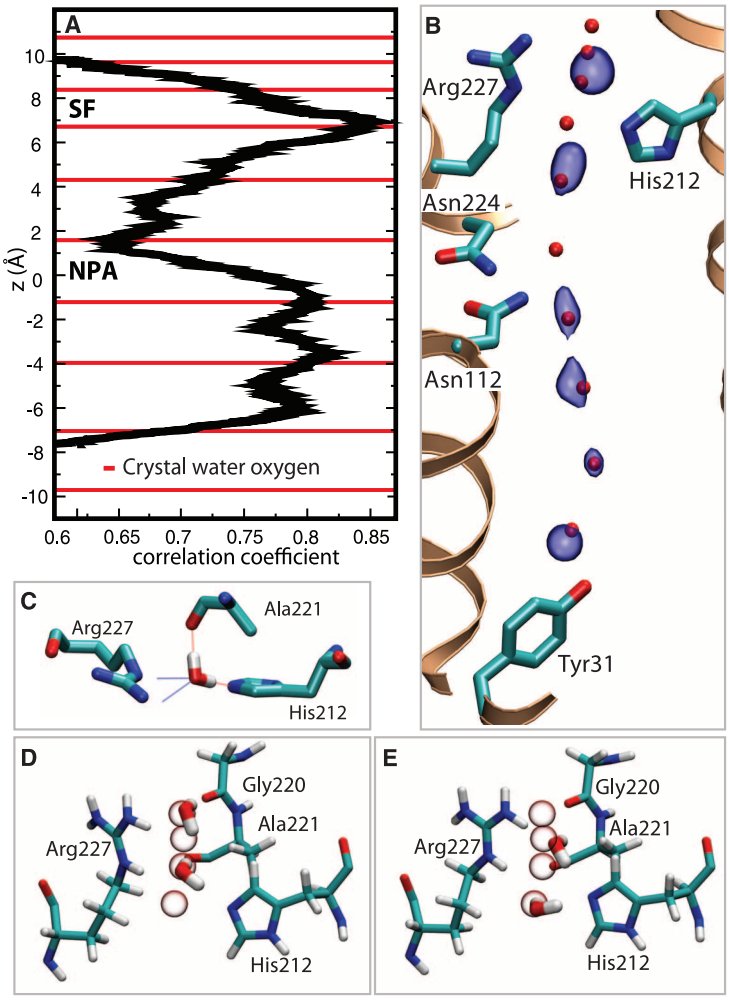

Fig. 4. Molecular dynamics simulations of water movements in Aqy1. (**A**) Plot illustrating the correlation of movements of adjacent water molecules. Strongly correlated movements arise in the SF and in the cytoplasmic half of the channel. The positions of oxygen atoms of crystallographic waters are indicated as red lines. (**B**) Surface representation (blue) of the most probable positions of water molecules (averaged over the final 15 ns of a 20-ns trajectory) superimposed on the crystallographic water positions (red spheres). (**C**) Snapshot of a water molecule within the SF with all four H-bond interactions occupied. (**D** and **E**) Snapshots corresponding to 1,3 and 2,4 water occupancy of the SF, which indicate the pair-wise movement of water molecules in this region. All four closely spaced SF crystallographic water positions are indicated as white spheres.

outside of the SF is weak. Correlated motions within the cytoplasmic half of the channel emerge from well-defined water-water H-bond interactions (Fig. 2C), whereas the correlations observed within the SF appear to be dictated by protein-water H-bond interactions. In addition to electrostatic effects, a disruption of the highly constrained SF water structure (Fig. 3) can explain why the mechanism of proton exclusion is sensitive to mutation of the conserved SF arginine and histidine residues (*27*, *28*). These findings illustrate how evolution has fine-tuned the water channel geometry so as to optimize protein function, suppressing proton transport without compromising water flux.

References and Notes

1. L. S. King, D. Kozono, P. Agre, *Nat. Rev. Mol. Cell Biol.* **5**, 687 (2004).
2. C. J. T. de Grotthuss, *Ann. Chim.* **58**, 54 (1806).
3. D. Marx, *ChemPhysChem* **7**, 1848 (2006).
4. D. Fu *et al.*, *Science* **290**, 481 (2000).
5. D. F. Savage, P. F. Egea, Y. Robles-Colmenares, J. D. O'Connell 3rd, R. M. Stroud, *PLoS Biol.* **1**, e72 (2003).
6. J. K. Lee *et al.*, *Proc. Natl. Acad. Sci. U.S.A.* **102**, 18932 (2005).
7. G. Fischer *et al.*, *PLoS Biol.* **7**, e1000130 (2009).
8. Z. E. Newby *et al.*, *Nat. Struct. Mol. Biol.* **15**, 619 (2008).
9. S. Törnroth-Horsefield *et al.*, *Nature* **439**, 688 (2006).
10. H. Sui, B. G. Han, J. K. Lee, P. Walian, B. K. Jap, *Nature* **414**, 872 (2001).
11. W. E. Harries, D. Akhavan, L. J. Miercke, S. Khademi, R. M. Stroud, *Proc. Natl. Acad. Sci. U.S.A.* **101**, 14045 (2004).
12. T. Gonen, P. Sliz, J. Kistler, Y. Cheng, T. Walz, *Nature* **429**, 193 (2004).
13. K. Murata *et al.*, *Nature* **407**, 599 (2000).
14. R. Horsefield *et al.*, *Proc. Natl. Acad. Sci. U.S.A.* **105**, 13327 (2008).
15. J. D. Ho *et al.*, *Proc. Natl. Acad. Sci. U.S.A.* **106**, 7437 (2009).
16. Y. Wang, K. Schulten, E. Tajkhorshid, *Structure* **13**, 1107 (2005).
17. E. Tajkhorshid *et al.*, *Science* **296**, 525 (2002).
18. B. L. de Groot, H. Grubmüller, *Science* **294**, 2353 (2001).
19. B. Ilan, E. Tajkhorshid, K. Schulten, G. A. Voth, *Proteins* **55**, 223 (2004).
20. N. Chakrabarti, E. Tajkhorshid, B. Roux, R. Pomès, *Structure* **12**, 65 (2004).
21. B. L. de Groot, T. Frigato, V. Helms, H. Grubmüller, *J. Mol. Biol.* **333**, 279 (2003).
22. M. O. Jensen, E. Tajkhorshid, K. Schulten, *Biophys. J.* **85**, 2884 (2003).
23. B. L. de Groot, H. Grubmüller, *Curr. Opin. Struct. Biol.* **15**, 176 (2005).
24. A. Burykin, A. Warshel, *Biophys. J.* **85**, 3696 (2003).
25. B. Wu, C. Steinbronn, M. Alsterfjord, T. Zeuthen, E. Beitz, *EMBO J.* **28**, 2188 (2009).
26. D. Wree, B. Wu, T. Zeuthen, E. Beitz, *FEBS J.* **278**, 740 (2011).
27. E. Beitz, B. Wu, L. M. Holm, J. E. Schultz, T. Zeuthen, *Proc. Natl. Acad. Sci. U.S.A.* **103**, 269 (2006).
28. H. Li *et al.*, *J. Mol. Biol.* **407**, 607 (2011).
29. Materials and methods are available as supplementary materials on *Science* Online.
30. Y. Zhou, J. H. Morais-Cabral, A. Kaufman, R. MacKinnon, *Nature* **414**, 43 (2001).
31. J. H. Morais-Cabral, Y. Zhou, R. MacKinnon, *Nature* **414**, 37 (2001).

Acknowledgments: Financial support is acknowledged from the European Union Integrated Project EDICT and the Marie Curie Training Network Aqua(glycero)porins, the Olle Engkvist Foundation, the Swedish Research Council, and NIH (grants R01-GM086749, U54-GM087519, and P41-GM104601). All simulations were performed using XSEDE resources at NSF supercomputing centers (grant MCA06N060). We thank staff of beamline ID29 of the ESRF for assistance during data collection and Karin Rödstrom for setting up crystallization plates at the ESRF in advance of data collection. The authors have made the following contributions: G.F., U.K.E., and R.N. conceived and designed the experiments; G.F. and U.K.E. performed the experiments; G.F., R.F., and U.K.E. analyzed the crystallographic data; G.E. and E.T. conceived and designed the MD simulations; and G.E. performed and analyzed the simulations. All authors contributed to writing the manuscript. Coordinates and structure factors have been deposited in the Protein Data Bank with accession number 3zoj.

Supplementary Materials

www.sciencemag.org/cgi/content/full/340/6138/1346/DC1
Materials and Methods
Figs. S1 to S5
Tables S1 and S2
References (*32*–*49*)

19 December 2012; accepted 24 April 2013
10.1126/science.1234306